Düzce University
Journal of Science & Technology

Research Article

Prediction of Deep Drawing Ratio for DP800 Steel by Using Modified-Mohr-Coulomb Damage Criteria

Elifnaz BABA[a], Nuri ŞEN[*a] Tolgahan CİVEK[a]

[a] *Department of Mechanical Engineering, Faculty of Engineering, Düzce University, Düzce, TURKEY*
* *Corresponding author's e-mail address: nurisen@duzce.edu.tr*
DOI: 10.29130/dubited.1610838

ABSTRACT

The demand for low-cost production in vehicle manufacturing while complying with the safety and environmental regulations is an enormous challenge. To comply with these challenges, sheet metal forming industries now extensively use advanced high-strength steels (AHSSs) in their products. However, due to excellent strength levels of AHSSs, problems arising in their forming stage, such as large spring-back and fracture, hinder the manufacturing process. At this stage, implementing finite element analysis (FEA) in the design processes greatly improves manufacturing processes since it allows determining possible forming errors before the actual forming process. In this study, the formability of DP800 steel has been investigated by carrying out deep drawing experiments. For that, a series of circular sheet metals, whose diameters were incrementally increased, have been deep drawn to a cup shape to determine the limiting drawing ratio (LDR). Additionally, Modified Mohr-Coulomb damage model has been utilised to predict the LDR in FEA. It has been found that the LDR of DP800 is 2.13 and the implemented damage model can successfully predict the LDR within only 2.35% error.

Keywords: *DP800 steel, Deep drawing ratio, Finite element analysis, Damage,*

Modified- Mohr Coulomb Hasar Kriteri Kullanılarak DP800 Çeliğinin Derin Çekme Oranının Tahmini

ÖZET

Araç imalatında güvenlik ve çevre düzenlemelerine uyum sağlarken düşük maliyetli üretim talebi muazzam bir zorluktur. Bu zorluklara uyum sağlamak için, sac metal şekillendirme endüstrileri artık ürünlerinde yaygın olarak gelişmiş yüksek dayanımlı çelikler (AHSS'ler) kullanmaktadır. Ancak, AHSS'lerin mükemmel dayanım seviyeleri nedeniyle, büyük geri yaylanma ve kırılma gibi şekillendirme aşamalarında ortaya çıkan sorunlar üretim sürecini engellemektedir. Bu aşamada, tasarım süreçlerinde sonlu elemanlar analizinin (FEA) uygulanması, gerçek şekillendirme sürecinden önce olası şekillendirme hatalarının belirlenmesine olanak tanıdığı için üretim süreçlerini büyük ölçüde iyileştirmektedir. Bu çalışmada, derin çekme deneyleri gerçekleştirilerek DP800 çeliğinin şekillendirilebilirliği araştırılmıştır. Bunun için, çapları kademeli olarak artırılan bir dizi dairesel sac metal, derin çekme oranını (LDR) belirlemek için bardak formunda derin çekilmiştir. Ek olarak, Değiştirilmiş Mohr-Coulomb hasar modeli, FEA'daki LDR'yi tahmin etmek için kullanılmıştır. DP800'ün LDR'sinin 2.13 olduğu ve uygulanan hasar modelinin LDR'yi sadece %2.35 hata payıyla başarılı bir şekilde tahmin edebildiği bulunmuştur.

Anahtar Kelimeler: *DP800 Çeliği, Derin çekme oranı, Sonlu elemanlar analizi, Hasar*

Received: 31/12/2024, Revised: 03/01/2025, Accepted: 13/01/2025

I. INTRODUCTION

Nowadays, with the shortage of fossil fuel resources and high level of vehicle usage which is undoubtfully one of the most reasons for environmental pollution and global warming, car manufacturers have mostly been seeking innovative and cost-effective solutions [1]. To address these big challenges, the weigh-lightened car concept is increasingly attracting attention in the sector. Therefore, many claim that the adoption of low-mass vehicles with a sustainable ecological and economical approach replacing the conventional structural steels will be an inevitable production method of next-generation cars. However, this production concept requires massive study in terms of realization of light weight car body pars under experimental conditions. In the fabrication of these new concept cars with light body parts, high-strength steels such as dual phase and trip steels play an important role. On the other hand, high-strength steels have some obvious disadvantages related to micromechanical responses to forming conditions making them highly challenging when applied as body parts. The formability is quite lower and the springback behaviour is considerably higher for high-strength steels as compared to the traditional steels [2]–[7]. Yet, to reach the similar level of safety for passengers traditional steel alloys force car manufacturers to increase the thickness of sheet metal on body parts causing environmental concerns and disadvantage relating to production costs. However, with around two times higher strength and yield point, AHSSs such as dual phase (DP) and complex phase (CP) steels, these challenges can be overcome depending on reliable and feasible metal forming technology.

Deep drawing is one of the most important fabrication processes among sheet metal forming phenomena in the car industry. Product quality is closely related to process parameters such as strain rate, blank holder force, punch speed, friction, tool geometry, process temperature and so on [8]. The success or failure of the fabrication of sheet metal part is largely affected by each of the factors. Thus, a deep understanding of drawing process is necessary to achieve desired flawless and various sheet metal car components.

FEA is a powerful tool that can be used in observing the effects of each forming parameter on the forming process without needing to manufacture the actual dies and the incessant trial-errors [9], [10]. However, in modelling of FEAs, it is important that the sheet metal is carefully characterized and some of the valuable aspects such as flow model and the damage model need to be thoroughly optimized [11]–[13]. Damage models in FEAs are used to examine the regions of the sheet metal where fractures are likely to occur. Damage models can be implemented in the FEAs as coupled and un-coupled models [14]–[18]. While the coupled damage models degrade the flow stress by linking the damage to the flow stress, in uncoupled damage models, damage does not affect the flow stress of the material. Although coupled models are considered to improve the accuracy of the predictions of the FEA, the amount of time needed to optimize their parameters can be quite exhaustive [18]. It is widely known that stress triaxiality is one of the most important parameters that significantly affects the formability of sheet metal. Thus, many damage models can be found in the literature such as Johnson Cook [19], Modified Mohr-Coulomb [20], Hosford-Coulomb [21], which links the damage to the stress triaxiality. However, in recent years, studies have shown that the Lode angle parameter has also have a significant impact on the formability of the sheet metals [22], [23]**.** Thus damage models that take into consideration of the stress triaxiality and as well as the Lode angle parameter such as Modified Mohr-Coulomb model have been started to be extensively used.

In this study, the formability of DP800 steel has been investigated by deep drawing experiments. Deep drawing experiments have been carried out for different blank diameters to determine the LDR of the DP800 steel. In addition, Modified Mohr-Coulomb damage model parameters have been optimized for the DP800 steel and used to predict the experimentally determined LDR in FEA.

II. MATERIALS AND METHODS

A. *Materials*

In this study, a cold rolled and tempered DP800 steel with a thickness of 1 mm was used. The chemical composition of the steel is listed Table 1. To investigate the mechanical properties of the sheet metal and to calibrate the damage model for the FEA, tensile test specimens (uniaxial, plane strain and shear) were cut along the rolling direction of the sheet metal. The geometrical dimensions of the tensile test specimens are shown in Figure 1. For the deep drawing experiments, circular blanks with different diameters (68, 70, 72, 74, 76, 78, 80 and 82 mm) were cut. All the specimens were cut with the aid of a water jet to avoid temperature influence on mechanical properties and the influence of edge effects resulting from poor cutting.

Table 1. Chemical composition of DP800 specimens

Sample	**Elemental composition *(wt.%)***							
	C	**Si**	**Mn**	**P**	**S**	**Al**	**Nb**	**Ti**
DP800	0.141	0.214	1.483	0.0106	0.0156	0.085	0.018	0.009

a)
b)
c)

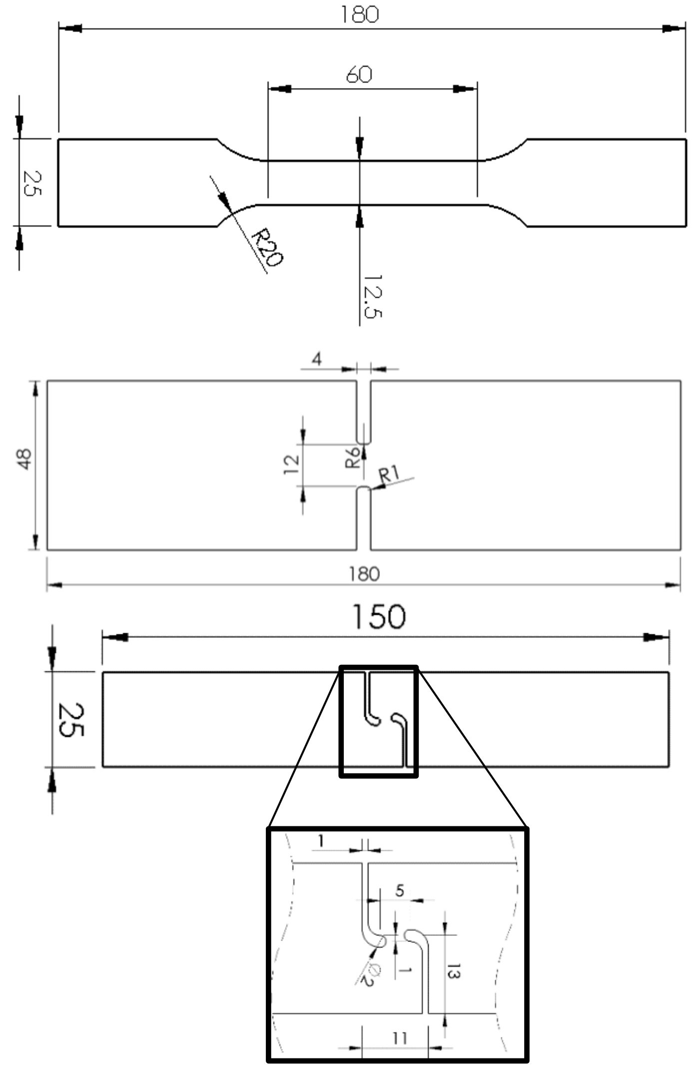

Figure 1. The dimensions of the tensile test specimens **a)** Uniaxial, **b)** Plane strain, **c)** Shear

B. *Mechanical Properties*

To examine the mechanical properties of the DP800 steel, uniaxial tensile tests were performed at three different velocities (0.11 mm/s, 1.1 mm/s, 10 mm/s). The tensile tests were carried out using the Zwick/Roell tensile testing machine. During the tests, the strain data were recorded by a video extensometer. The tensile stress–strain graphs are shown in Figure 2., and the obtained mechanical properties are given in Table 2. As shown in Figure 2., the strain rate effect has not had a significant impact on the tensile strength of the DP800 steel. However, the increase in the strain rate has had a slightly reducing impact on the total elongation. In order to acquire the anisotropic coefficients of the DP800 steel, uniaxial tensile tests were carried out along the rolling direction (RD), diagonal direction (DD) and transverse direction (TD) of the sheet metal. The obtained Lankford coefficients were as; $\mathbf{r_0}$= 0.83, $\mathbf{r_{45}}$=1.00, $\mathbf{r_{90}}$= 1.01. The tensile stress-strain graphs along the RD, DD, and TD of the sheet metal are shown in Figure 3**.**

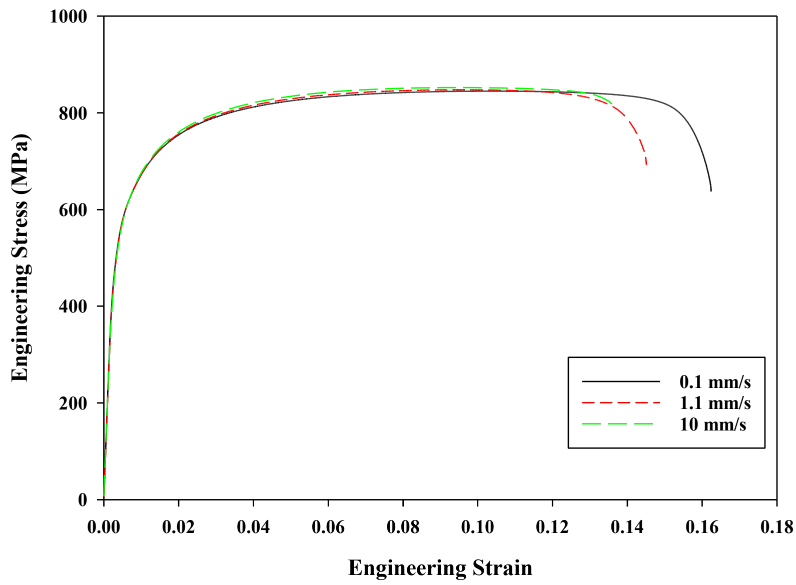

Figure 2. The tensile stress – strain graphs of DP800 steel

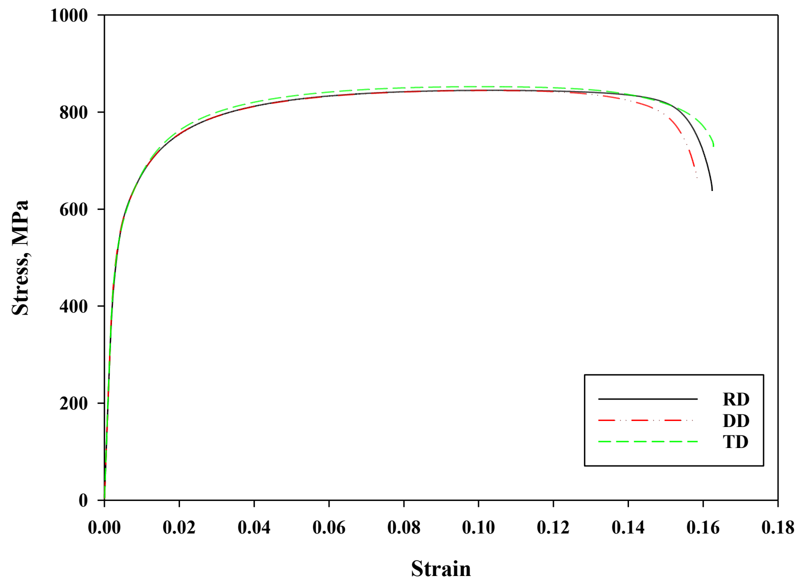

Figure 3. The tensile stress – strain graphs along the RD, DD, and TD of DP800 steel

Table 2. The mechanical properties of DP800 steel

Mechanical Properties	Test Velocity *(mm/s)*		
	0.1	**1.1**	**10**
Yield Stress *(MPa)*	566	571	564
Tensile Stress *(MPa)*	845	848	852
Uniform Elongation	0.10	0.09	0.09
Total Elongation	0.16	0.14	0.14

C. *The FEA Models for the Tensile Test Simulations*

This study used the FEA to estimate the deep drawing ratio and the thickness distributions of the drawn parts. Simufact Forming 2024.1 FEA simulation software was used to carry out the analysis.To do this, the parameters of the hardening model (Section D.) and the damage model (Section E.) need to be optimised. Hence, three different tensile test specimens (uniaxial, plane strain and shear) were modelled as shown in Figure 4. The models were meshed with 0.6 mm hexahedral elements and the mesh along the test specimens' deformation regions were refined twice. Three elements were used over the thickness direction of the specimens. In the models, the test specimens were placed in between the grips and glued to the grips by glue-type contact. The plane strain and shear specimens were stretched by the upward movement of the Grip1 with a 0.11 mm/s velocity. The uniaxial specimen, however, was stretched for three different velocities (0.11, 1.1 and 10 mm/s) as in the experiments to verify the accuracy of the hardening model parameters at each tension velocity.

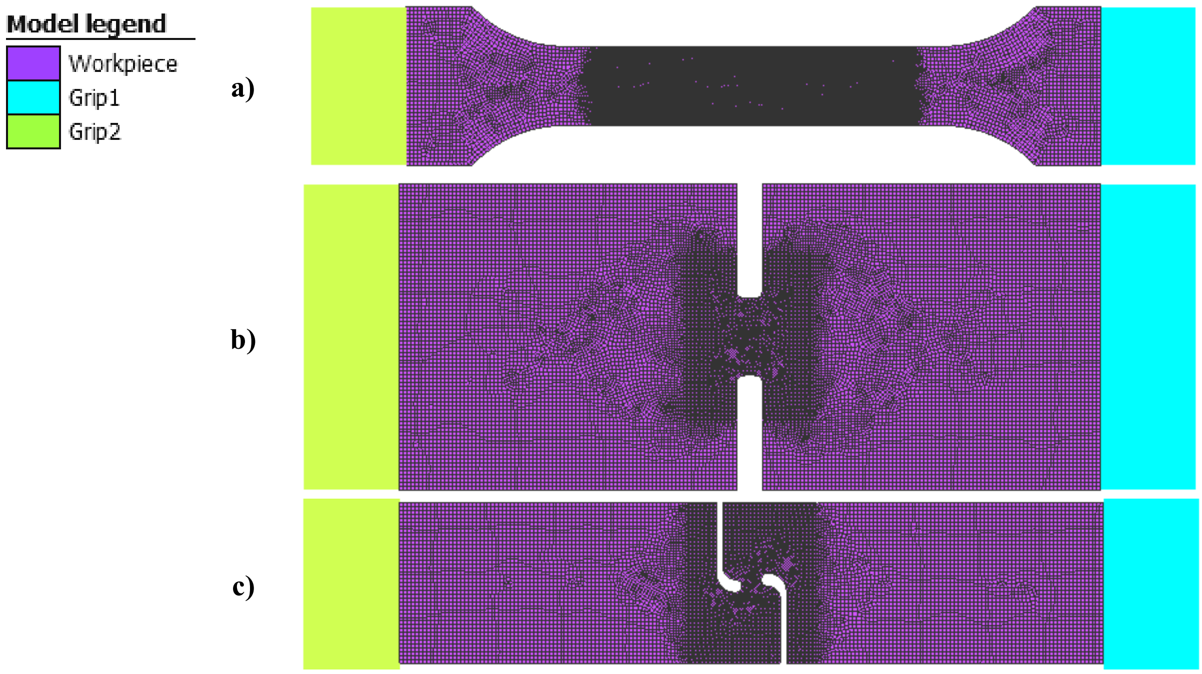

Figure 4. The FEA models of the tensile test specimens **a)** uniaxial, **b)** plane strain, **c)** shear

D. ***The calibration of the hardening model***

During the tensile testing of sheet metals only a small fraction of uniform elongation could be obtained, however, during actual stamping or drawing applications, larger strain values may occur during the forming stage [24]. To overcome this issue, the obtained flow strain from the uniaxial tensile test is extrapolated up to a certain strain value by a determined hardening model. In this study, Hollomon hardening model, given in Equation 1., was used to extrapolate the flow stress of the DP800 steel. The model parameters, K, and, n, were initially determined from the slope of the logarithmic true stress and strain data. To calibrate the parameters of the hardening model, uniaxial tensile test simulations were run with the initial parameter values. The obtained force-displacement curves from the simulation were compared with the experimental force-displacement curves. The parameters were then updated until the force-displacement curves obtained from the simulation and experimental tests matched. The parameters of the hardening model are given in Table 3., and the force-displacement curves from the experimental and simulation results are shown in Figure 5. As can be seen in Figure 5., the obtained force-displacement curves from the simulation highly matched the experimental values.

$$\sigma = K\epsilon^{n} \tag{1}$$

Table 3. Hollomon hardening model parameters used in the simulations

Test velocity *(mm/s)*	**K**	**n**
0.11	1127	0.082
1.1	1132	0.08
10	1140	0.085

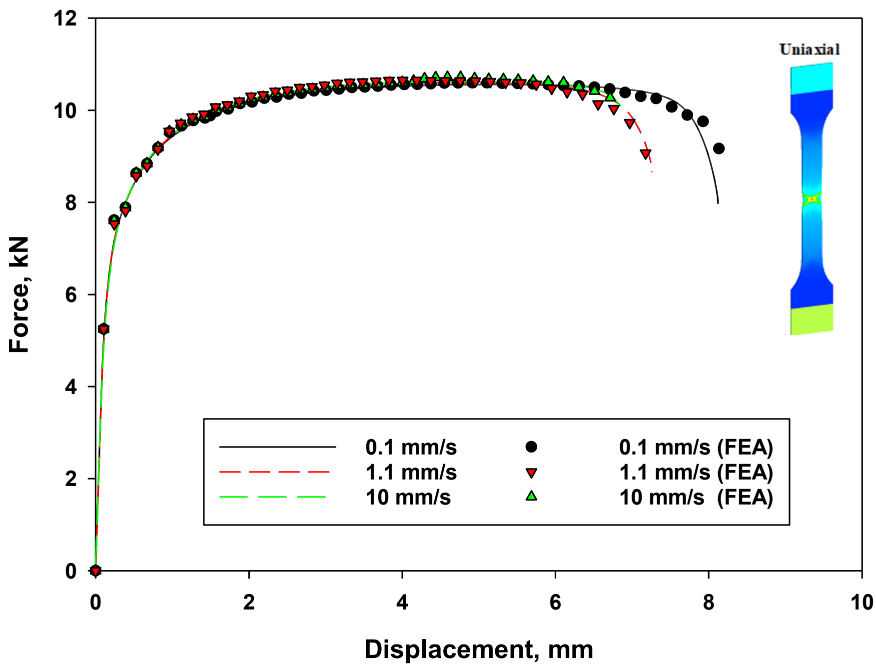

Figure 5. The comparison of the force-displacement curves obtained from the experimental and simulation results

E. ***The calibration of the damage model parameters***

In FEAs, various damage criterions could be used to observe the critical areas of the sheet metal, which are susceptible to fracture. Recently, uncoupled damage models such as Johnson-Cook or Modified Mohr-Coulomb are preferred in many studies due to their easier applicability as compared to the traditional forming limit diagram method [25], [26]. In this study, the uncoupled Modified Mohr-Coulomb damage model, given in Equation 2., was used to determine the LDR of the DP800 steel. To calibrate its parameters, the tensile test specimens, (uniaxial, plane strain, shear), were simulated up to the fracture displacement point. Then, the average stress triaxiality and lode angle parameter values were recorded at the critical elements where the strain was localised. The evolution of the stress triaxiality and lode angle parameter values are shown in Figure 6. The average values of stress triaxiality, lode angle parameter and the fracture strain values are given in Table 4. The average stress triaxiality, lode angle parameter and the fracture strain values were input into the parameter calibration tool existing in Simufact Forming 2024.1 and the 3D damage surface shown in Figure 7. were obtained. The parameters of the Modified Mohr-Coulomb damage model parameters are given in Table 5.

$$\bar{\epsilon}_f = \left\{\frac{A}{C_2}\left[C_\theta^s+\frac{\sqrt{3}}{2-\sqrt{3}}(C_\theta^{ax}-C_\theta^s)\left(\sec\left(\frac{\bar{\theta}\pi}{6}\right)-1\right)\right] x\sqrt{\frac{1+C_1^2}{3}}\ \cos\left(\frac{\bar{\theta}\pi}{6}\right)+c_1\left(\eta+\frac{1}{3}\sin\left(\frac{\bar{\theta}\pi}{6}\right)\right)\right\}^{-\frac{1}{n}} \qquad (2)$$

where η, σ_m and σ_{vM} represent the stress triaxiality, mean stress and von Mises stress, respectively. The notations shown as θ, ζ, and $\bar{\theta}$ represent the lode angle, normalized deviatoric invariant and Lode angle parameter, respectively. The notations given in Equation 11. **s**uch as $\bar{\epsilon_f}$, A, n, c_1, c_2, C_θ^s, C_θ^{ax} represent the parameters of MMC damage model. $\bar{\epsilon_f}$ denotes the failure strain, A and n represent the hardening coefficient and strain hardening exponent, respectively, c_1 describes the dependency of fracture strain on the stress triaxiality, c_2 influences the height of the fracture surface, C_θ^s describes the amount of lode angle dependency of the fracture surface, C_θ^{ax} controls the asymmetry of fracture surface with respect to Lode angle parameter and is taken as 1 for $\bar{\theta} > 0$.

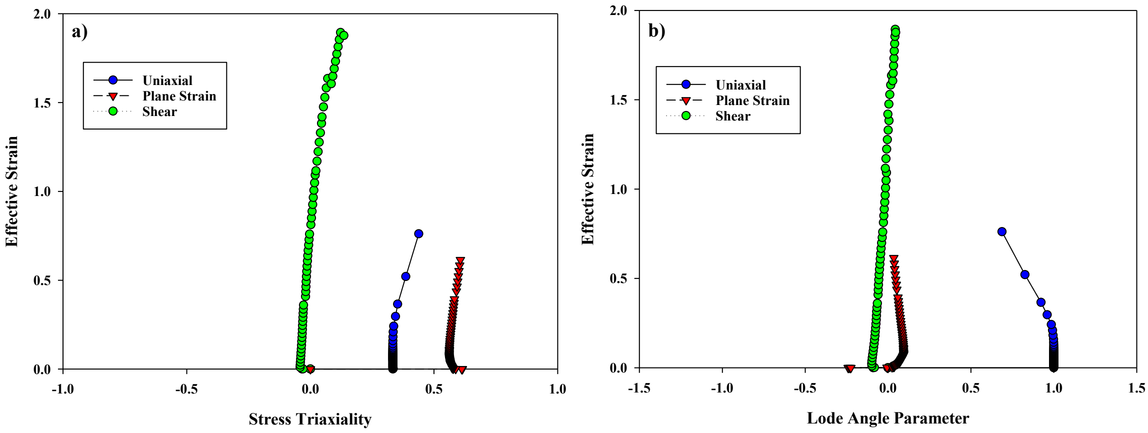

Figure 6. The evolution of the stress triaxiality and lode angle parameter values

Table 4. The average values of stress triaxiality, lode angle parameter and the fracture strain values

Test Specimen	Stress Triaxiality	Lode Angle Parameter	Fracture Strain
Uniaxial	0.33	1	0.76
Plane Strain	0.6	0.04	0.62
Shear	0	0	0.89

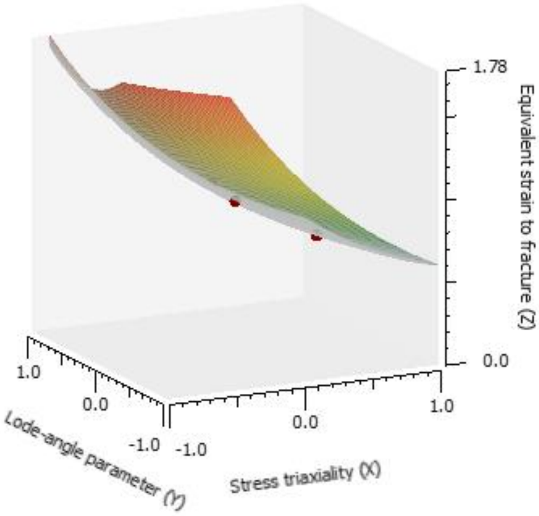

Figure 7. The Modified Mohr-Coulomb 3D damage surface

Table 5. The parameters of the Modified Mohr-Coulomb damage model

A	n	c_1	c_2	C_θ^s	C_θ^{ax}
1127	0.082	0.029	567.043	0.879	1

F. *Deep drawing experiments*

A double-acting hydraulic press (HDÇP 50/20 with 10+3 HP) was employed in the deep drawing experiments. The die setup for the deep drawing experiments is shown in Figure 8. H13 steel was used as the material for the die tools. The dimensions of the die tools are listed in Table 6. In the experiments, circular blanks were placed in the die cavity and then blank sheets were clamped between the die and blank holder that restricted the flow of material, thereby preventing wrinkles at the flange. The blankholder force used in the experiments was increased with the increase in the diameter of the blanks to prevent wrinkling of the sheet metal. Blankholder forces that were applied in the experiments for each blank diameter are listed in Table 7. Before carrying out the deep drawing experiments, graphite lubricant was sprayed on the specimens to reduce the friction between the die tools. To even further reduce the friction, a teflon film of 0.3 mm thickness was placed around the flange area of the sheet metal. The used lubricants for the deep drawing experiments are shown in Figure 9.

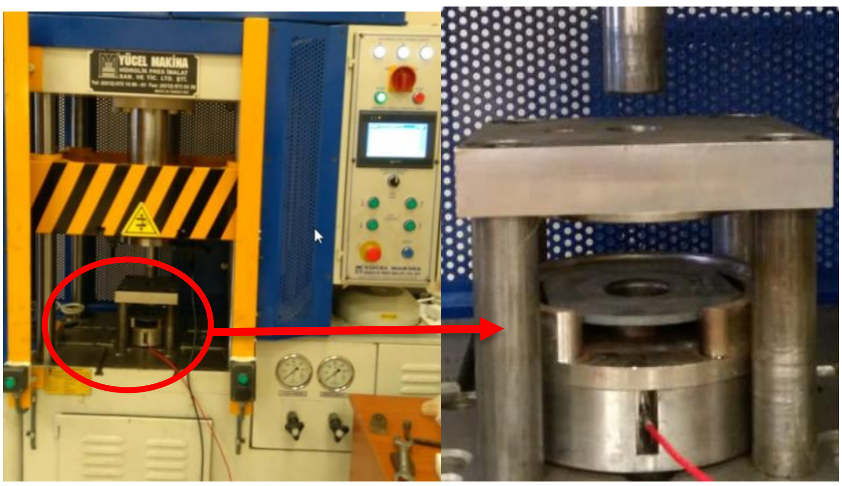

Figure 8. Experimental deep drawing die setup

Table 6. The dimensions of the die tools

Die tools	Dimensions *(mm)*
Punch	37.56
Die	39.98
Punch radius	5
Die radius	5

Table 7. The used blankholder force for different blank diameters in the deep drawing experiments

Blank diameter *(mm)*	Blankholder force *(tons)*
68	6
70	7
72	7
74	8
76	9
78	10
80	10
82	10

Figure 9. The used lubricants for the deep drawing experiments, **a)** Teflon film **b)** Graphite

G. ***FEA model for the deep drawing simulations***

For the simulation of the deep drawing experiments, simplistic models of the die tools were created and exported to the Simufact Forming software as shown in Figure 10. In the deep drawing model, die tools were chosen as rigid body parts, whereas the specimen was designated as a deformable body. Only 1/4 of the blank sheet was modelled in the simulations to reduce the calculation time. However, symmetry planes were used to simulate the full body of the sheet metal. The sheet specimens were meshed with hexahedral elements in 0.5 mm thickness and three elements were used over the thickness direction. The friction coefficient between the die tools and the sheet specimen was chosen as 0.04. Sigma-based Hill-48 yielding criterion was used in the simulations.

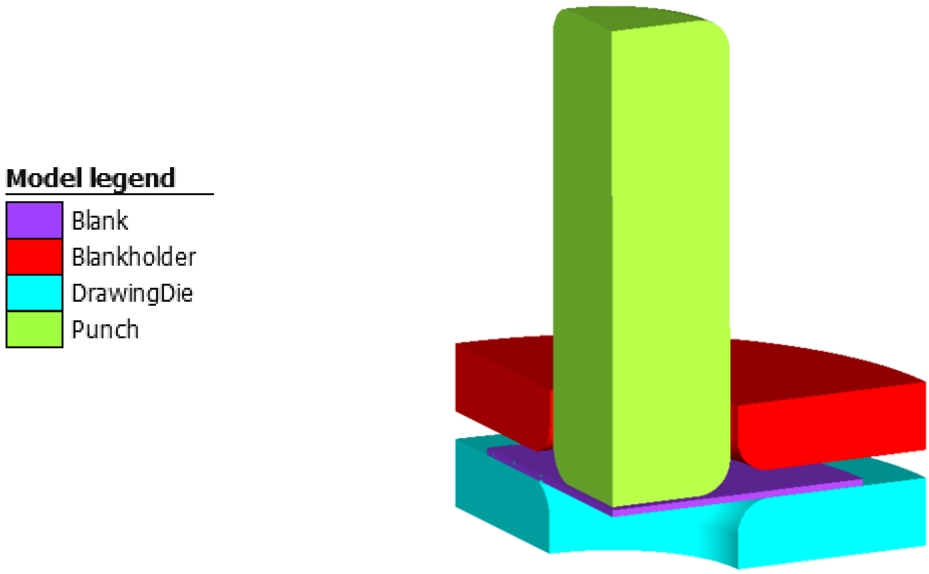

Figure 10. The deep drawing model for the FEA simulation

III. RESULTS AND DISCUSSIONS

A. ***MMC damage model***

During the forming stage of sheet metals, the process parameters such as friction, blankholder force, temperature etc., can influence the success of the forming process [8]. All these factors affect the formability of the material and determine how the material responds during the forming stage. Although there are far many properties that can influence the formability of sheet metals, the stress triaxiality factor is widely known that its increase causes significant reductions in the formability of sheet metals [27], [28] Another factor, known as Lode angle parameter, has also been shown by many studies to be an effective factor in the formability of sheet metals. Hence damage models that take into consideration of the influence of stress triaxiality and Lode angle parameters, such as MMC, are frequently preferred damage models to predict the fracture. In Figure 11., the simulated force-displacement curves of uniaxial, plane strain and shear tests, when the damage is activated, have been compared with the experimental results. It can be seen that the calibrated MMC damage model could precisely predict the final fracture point for each test. The initiation and the evolution of the fracture for uniaxial, plane strain and shear tests have been shown in Figures 12, 13 and 14, respectively. Earlier to the fracture initiation, the strain localised at the middle section of the uniaxial test specimen and the fracture initiated at this point. With further deformation, the fracture has spread through a 45^0 angle, which accurately resembles the experimental fracture surface. Similarly, the strain has localised along the middle section of the plane strain specimen and the fracture has initiated along this section, which then spread through the notches on both sides of the specimen. For the shear test specimen, the strain has localised along the mid-section of the shear area and the fracture has initiated in this section close to the notches, which then spread through the mid-section and completely fractured. It can be seen that the MMC damage model could precisely predict the final fracture point and the final fracture shape of the test specimens.

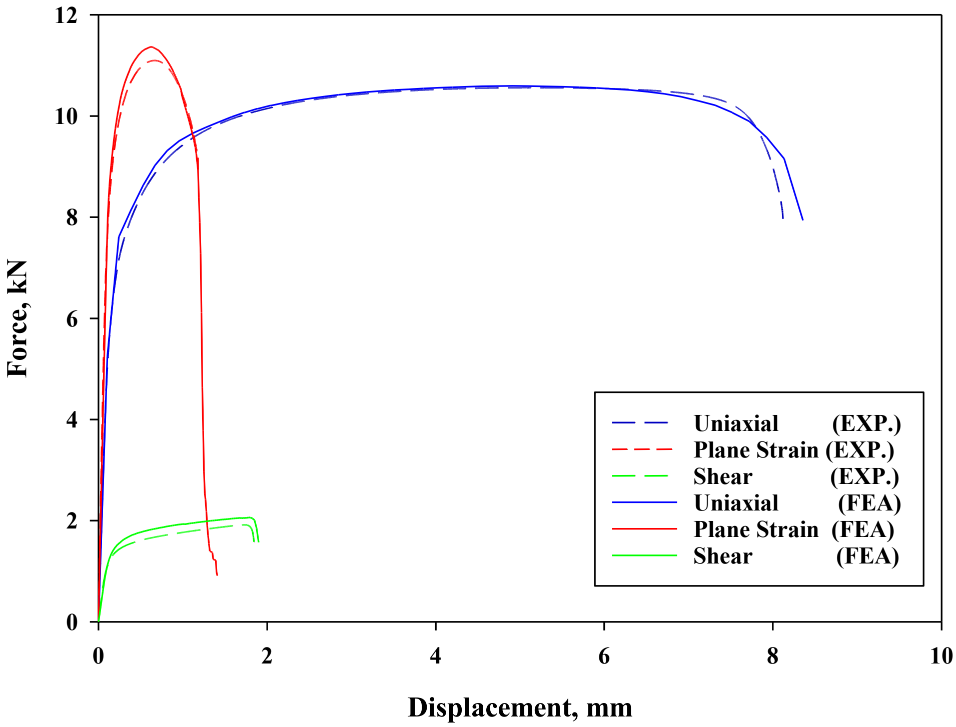

Figure 11. The comparisons of the experimental and simulated force-displacement curves for uniaxial, plane strain and shear tests

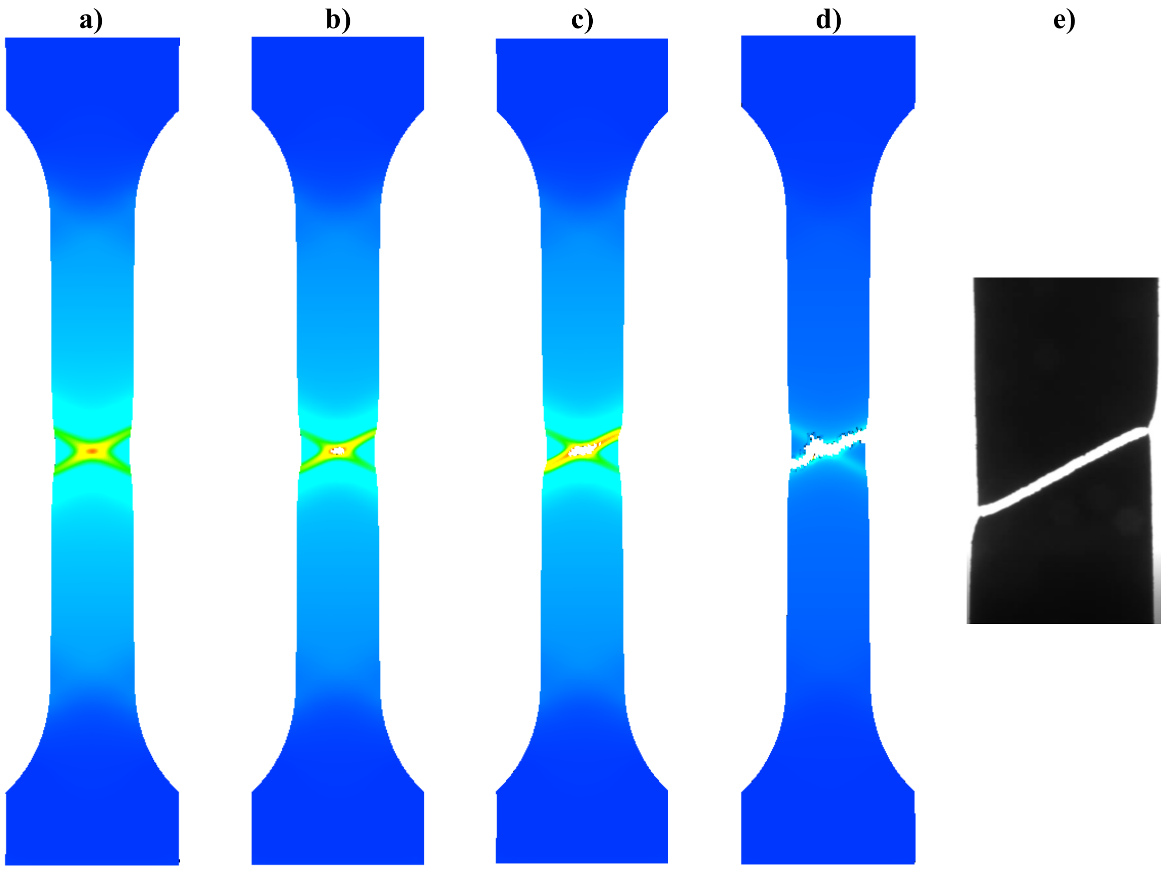

Figure 12. a) Strain localisation, **b)** fracture initiation, **c)** fracture evolution **d)** the final fracture predicted by the FEA and **e)** experimental fracture surface for uniaxial tensile test

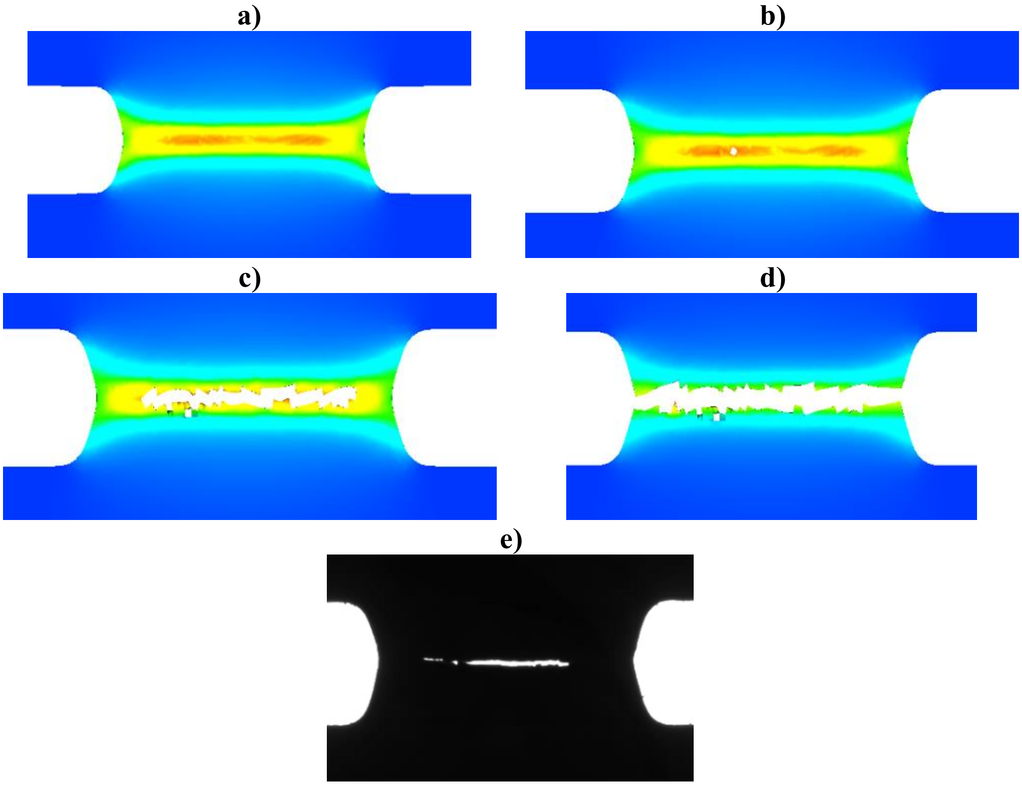

Figure 13. a) Strain localisation, **b)** fracture initiation, **c)** fracture evolution **d)** the final fracture predicted by the FEA and **e)** experimental fracture surface for plane strain test

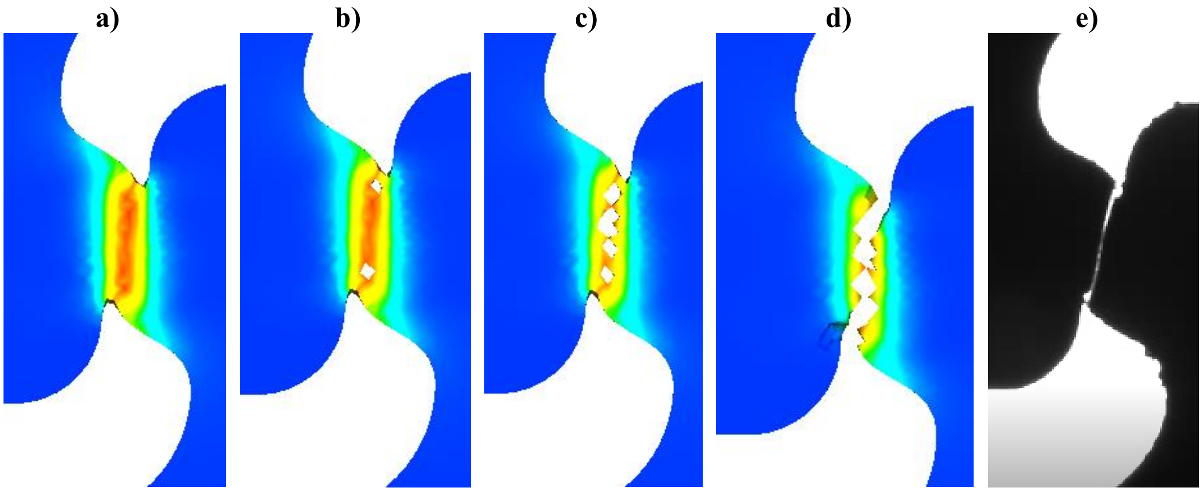

Figure 14. a) Strain localisation, **b)** fracture initiation, **c)** fracture evolution **d)** the final fracture predicted by the FEA and **e)** experimental fracture surface for shear test

B. ***Limiting Drawing Ratio Tests and Its Prediction by the FEA***

LDR is known as the ratio of the largest blank diameter, which can be successfully deep drawn, to the punch diameter by which the sheet metal is deep drawn [29], [30]. The LDR of sheet metal is one of the indicators that show the sheet metal's formability. Simply, it shows how deep a sheet metal can be successfully drawn. The LDR could determine whether a forming process could be completed without failure. Hence, its correct estimate by the FEA methods can indicate how well the damage model and the flow curve have been calibrated. The experimentally deep drawn DP800 steels have been shown in Figure 15. It can be seen that the DP800 steel could be deep drawn without failure up to 80 mm blank diameter, which corresponds to the LDR of 2.13. The sheet metal ruptured from the punch radius contact region, when the blank diameter was increased to 82 mm. It is known that the plane strain type of deformation strictly limits the forming limits. During the deep drawing process, plane strains form along the punch radius contact region, thus, failure occurs at this region of the sheet metal. In Figure 16., the deep drawing simulations of the DP800 steel can be seen. It can be seen that the sheet metal could be deep drawn up to 78 mm diameter without failure, corresponding to the LDR of 2.08. The sheet metal, ruptured from the punch radius contact region, when the blank diameter was increased to 80 mm. Thus, it is seen that the created FEA model has been conservative in its LDR estimation. The error between the experimental LDR and the FEA has been noted to be 2.35%. Hence, it is seen that the FEA model has been able to estimate the LDR precisely.

Figure 15. Experimentally deep drawn DP800 steels

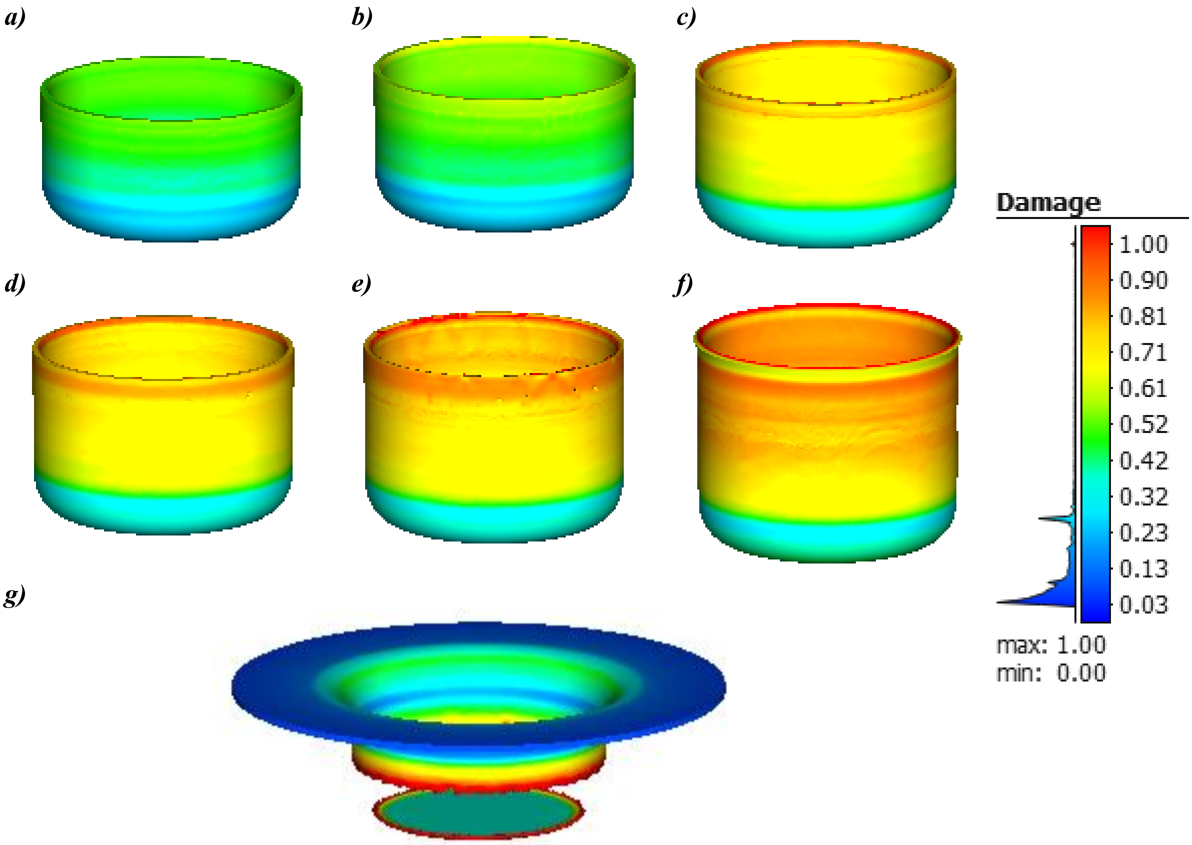

Figure 16. Deep drawing simulations of the DP800 steel

C. *Thickness Distributions*

In many forming processes, such as deep drawing, stamping or bending, the thickness of the formed body is desired to be uniformly distributed [31]–[33]. This uniform distribution of thickness is especially important when the formed part is expected to respond to the external forces similarly for each region of the part. If excessive thinning occurs during the forming stage of the part, a fracture is likely to form at this region of the part when it is in service. Thus, it is of paramount importance that excessive thinning does not occur, and that the thickness is uniformly distributed during the forming stage. In Figure 17., the measured and the predicted thickness distributions are shown. It can be seen that the parts have started thinning after the 2nd measurement point and that the amount of thinning has increased with the increase in the blank diameter. The minimum thickness has occurred at the 4th measurement point, which is the area where the sheet metal is exerted to plane strain deformation. As shown in Figure 17.a, the FEA has predicted a similar thickness distribution for each blank diameter. The percentage error between the predicted and the measured thickness is shown in Figure 18. It can be seen that the error values have been smaller than 6% and that the largest error has been 5.79% for 76 mm blank diameter.

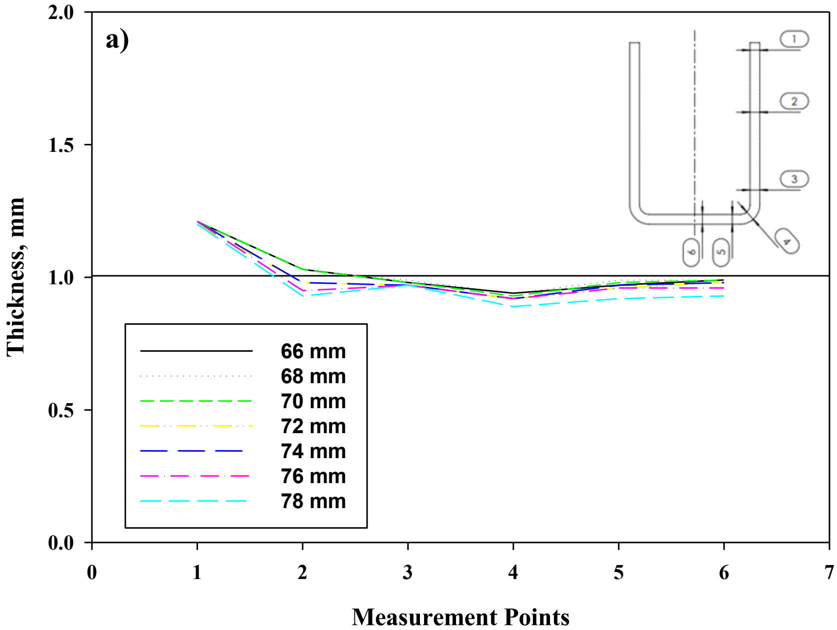

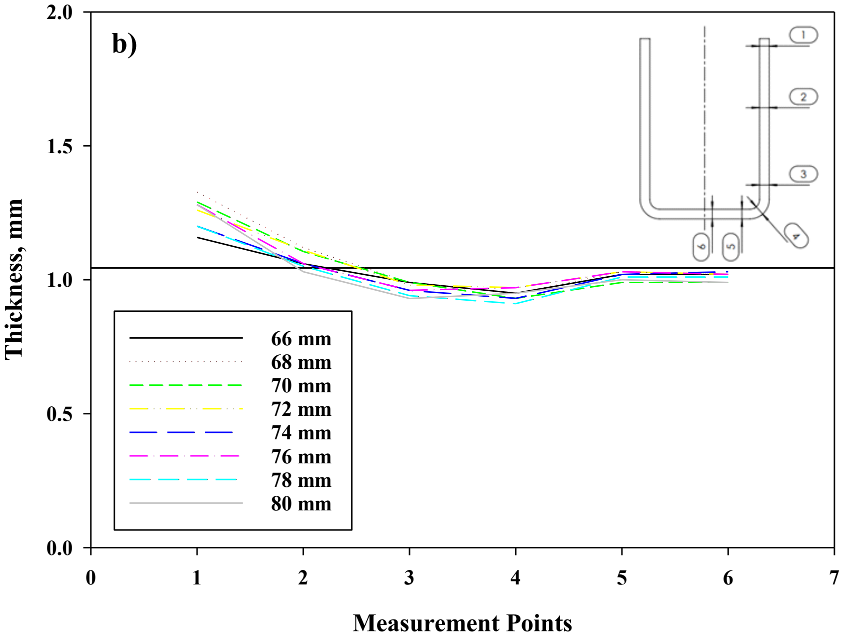

Figure 17. a) Predicted thickness distributions and **b)** experimental thickness distributions of the deep drawn parts

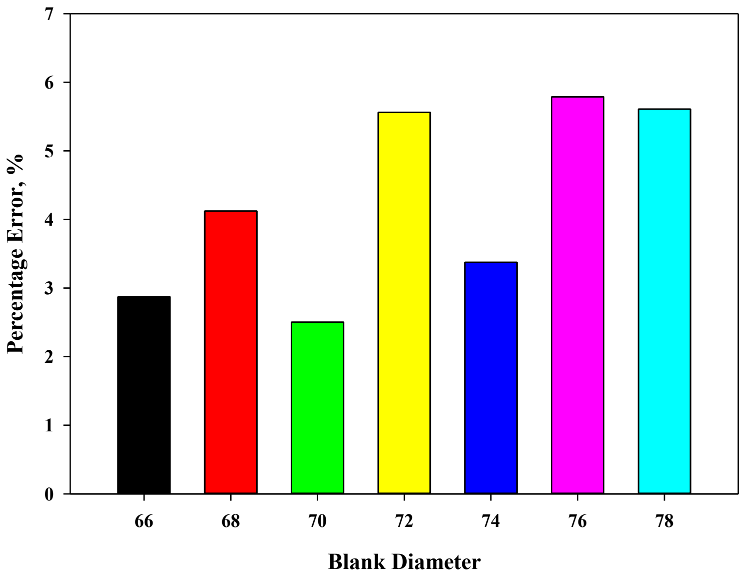

Figure 18. The percentage error level of the prediction of blank thickness for each blank diameter

IV. CONCLUSION

In this study, deep drawing experiments have been carried out for DP800 steel for different blank diameters to determine the LDR. Additionally, the LDR has been predicted by FEA using the Modified Mohr-Coulomb damage model. The main conclusions that can be drawn from the study are listed below:

- The calibrated Modified Mohr-Coulomb damage model have been able to precisely predict the final fracture displacements for uniaxial, plane strain and shear test specimens.
- The calibrated Hollomon hardening model has been successful in its force – displacement predictions for uniaxial, plane strain and shear test specimens.
- The LDR of DP800 steel have been experimentally found to be 2.13.
- The FEA model has predicted the LDR as 2.08, which is only 2.35% off from the experimentally obtained LDR
- The FEA model has been able to predict the experimentally measured thickness distribution under 6% error.

V. REFERENCES

[1] S. Mahabunphachai and M. Koç, "Investigations on forming of aluminum 5052 and 6061 sheet alloys at warm temperatures," *Mater. Des.*, vol. 31, no. 5, pp. 2422–2434, 2010, doi: https://doi.org/10.1016/j.matdes.2009.11.053.

[2] H. Lim, M. G. Lee, J. H. Sung, J. H. Kim, and R. H. Wagoner, "Time-dependent springback of advanced high strength steels," *Int. J. Plast.*, vol. 29, no. 1, pp. 42–59, 2012, doi: 10.1016/j.ijplas.2011.07.008.

[3] P. Chen and M. Koç, "Simulation of springback variation in forming of advanced high strength steels," *J. Mater. Process. Technol.*, vol. 190, no. 1–3, pp. 189–198, 2007, doi: 10.1016/j.jmatprotec.2007.02.046.

[4] W. Gan, S. S. Babu, N. Kapustka, and R. H. Wagoner, "Microstructural effects on the springback of advanced high-strength steel," *Metall. Mater. Trans. A*, vol. 37, pp. 3221–3231, 2006.

[5] S. Panich, F. Barlat, V. Uthaisangsuk, S. Suranuntchai, and S. Jirathearanat, "Experimental and

theoretical formability analysis using strain and stress based forming limit diagram for advanced high strength steels," *Mater. Des.*, vol. 51, pp. 756–766, 2013, doi: https://doi.org/10.1016/j.matdes.2013.04.080.

[6] Ö. N. Cora and M. Koç, "Promises and Problems of Ultra/Advanced High Strength Steel (U/AHSS) Utilization in Automotive Industry," *7th Automot. Technol. Congr. (OTEKON 2014)*, no. November, pp. 1–8, 2014, doi: 10.13140/2.1.4725.0883.

[7] N. Baluch, Z. M. Udin, and C. S. Abdullah, "Advanced high strength steel in auto industry: an overview," *Eng. Technol. Appl. Sci. Res.*, vol. 4, no. 4, pp. 686–689, 2014.

[8] C. P. Singh and G. Agnihotri, "Study of deep drawing process parameters: a review," *Int. J. Sci. Res. Publ.*, vol. 5, no. 2, pp. 1–15, 2015.

[9] N. Şen and Y. Baykal, "Development of car wishbone using sheet metal tearing process via the theory of inventive problem-solving (TRIZ) method," *J. Brazilian Soc. Mech. Sci. Eng.*, vol. 41, no. 10, pp. 1–10, 2019, doi: 10.1007/s40430-019-1884-7.

[10] Ö. Şenol, V. Esat, and H. Darendeliler, "Springback analysis in air bending process through experiment based artificial neural networks," *Procedia Eng.*, vol. 81, no. October, pp. 999–1004, 2014, doi: 10.1016/j.proeng.2014.10.131.

[11] M. Aghaei and S. Ziaei-Rad, "A micro mechanical study on DP600 steel under tensile loading using Lemaitre damage model coupled with combined hardening," *Mater. Sci. Eng. A*, vol. 772, no. September 2019, p. 138774, 2020, doi: 10.1016/j.msea.2019.138774.

[12] S. Abbasnejad Dizaji, H. Darendeliler, and B. Kaftanoğlu, "Effect of hardening models on different ductile fracture criteria in sheet metal forming," *Int. J. Mater. Form.*, vol. 9, no. 3, pp. 261–267, 2016, doi: 10.1007/s12289-014-1188-5.

[13] K. Ahn and M. H. Seo, "Effect of anisotropy and differential work hardening on the failure prediction of AZ31B magnesium sheet at room temperature," *Int. J. Solids Struct.*, vol. 138, pp. 181–192, 2018, doi: 10.1016/j.ijsolstr.2018.01.011.

[14] R. Li, Z. Zheng, M. Zhan, H. Zhang, and Y. Lei, "A comparative study of three forms of an uncoupled damage model as fracture judgment for thin-walled metal sheets," *Thin-Walled Struct.*, vol. 169, no. August, p. 108321, 2021, doi: 10.1016/j.tws.2021.108321.

[15] R. Billardon and L. Moret-Bailly, "Fully coupled strain and damage finite element analysis of ductile fracture," *Nucl. Eng. Des.*, vol. 105, no. 1, pp. 43–49, 1987.

[16] C. Soyarslan and A. E. Tekkaya, "A damage coupled orthotropic finite plasticity model for sheet metal forming: CDM approach," *Comput. Mater. Sci.*, vol. 48, no. 1, pp. 150–165, 2010.

[17] C. Y. Tang, J. P. Fan, and T. C. Lee, "Simulation of necking using a damage coupled finite element method," *J. Mater. Process. Technol.*, vol. 139, no. 1–3, pp. 510–513, 2003.

[18] P.-O. Bouchard, L. Bourgeon, S. Fayolle, and K. Mocellin, "An enhanced Lemaitre model formulation for materials processing damage computation," *Int. J. Mater. Form.*, vol. 4, pp. 299–315, 2011.

[19] M. E. Korkmaz, "Verification of Johnson-Cook parameters of ferritic stainless steel by drilling process: experimental and finite element simulations," *J. Mater. Res. Technol.*, vol. 9, no. 3, pp. 6322–6330, 2020.

[20] H. Talebi-Ghadikolaee, H. Moslemi Naeini, M. J. Mirnia, M. A. Mirzai, S. Alexandrov, and H. Gorji, "Experimental and numerical investigation of failure during bending of AA6061 aluminum alloy sheet using the modified Mohr-Coulomb fracture criterion," *Int. J. Adv. Manuf. Technol.*, vol. 105, pp. 5217–5237, 2019.

[21] M. B. Gorji and D. Mohr, "Predicting shear fracture of aluminum 6016-T4 during deep drawing: Combining Yld-2000 plasticity with Hosford–Coulomb fracture model," *Int. J. Mech. Sci.*, vol. 137, pp. 105–120, 2018.

[22] Y. Bao, "Dependence of ductile crack formation in tensile tests on stress triaxiality, stress and strain ratios," *Eng. Fract. Mech.*, vol. 72, no. 4, pp. 505–522, 2005.

[23] T. Güzelderen and H. Darendeliler, "Effects of triaxiality and lode parameter on deep drawing process," *Mater. Res. Proc.*, vol. 41, 2024.

[24] J. Mulder, H. Vegter, H. Aretz, S. Keller, and A. H. Van Den Boogaard, "Accurate determination of flow curves using the bulge test with optical measuring systems," *J. Mater. Process. Technol.*, vol. 226, pp. 169–187, 2015.

[25] A. F. Ávila and E. L. S. Vieira, "Proposing a better forming limit diagram prediction: a comparative study," *J. Mater. Process. Technol.*, vol. 141, no. 1, pp. 101–108, 2003, doi: https://doi.org/10.1016/S0924-0136(03)00162-6.

[26] S. P. S. S. Sivam, N. Harshavardhana, and R. Rajendran, "Artificial Neural Network prediction of forming limit diagram for directionally-rolled, size scaled copper strips," *Proc. Inst. Mech. Eng. Part C J. Mech. Eng. Sci.*, vol. 238, no. 8, pp. 3299–3307, 2024, doi: 10.1177/09544062231184396.

[27] A. J. Martínez-Donaire, M. Borrego, D. Morales-Palma, G. Centeno, and C. Vallellano, "Analysis of the influence of stress triaxiality on formability of hole-flanging by single-stage SPIF," *Int. J. Mech. Sci.*, vol. 151, pp. 76–84, 2019.

[28] T. Sjöberg, S. Marth, J. Kajberg, and H.-Å. Häggblad, "Experimental characterisation of the evolution of triaxiality stress state for sheet metal materials," *Eur. J. Mech.*, vol. 66, pp. 279–286, 2017.

[29] D.-K. Leu, "Prediction of the limiting drawing ratio and the maximum drawing load in cup-drawing," *Int. J. Mach. Tools Manuf.*, vol. 37, no. 2, pp. 201–213, 1997.

[30] D. Van Dinh, S. Van Nguyen, A. N. Pham, L. Van Nguyen, and V. D. Do, "Investigation and establishment of rational geometric factors of die in the deep drawing without a blank holder," *EUREKA Phys. Eng.*, no. 1, pp. 105–115, 2024.

[31] M. Colgan and J. Monaghan, "Deep drawing process: analysis and experiment," *J. Mater. Process. Technol.*, vol. 132, no. 1–3, pp. 35–41, 2003.

[32] W. Sun, W. Liu, and S. Yuan, "Suppressing wrinkles in thin-walled dome parts: A novel deep drawing method with active stress control," *J. Mater. Process. Technol.*, vol. 324, p. 118249, 2024.

[33] A. Taşkın and C. G. Dengiz, "Experimental and numerical optimization of deep drawing process parameters for square medical container design with the Taguchi method," *Int. J. Adv. Manuf. Technol.*, vol. 132, no. 5, pp. 2643–2659, 2024.